Common-path holographic interferometer for flatness testing

P. Jacquot*, X. Colonna de Lega* and P.M. Boone**

*Laboratory of stress analysis, Swiss Federal Institute of Technology,
CH – 1015 Lausanne

**Laboratory Soete for strength of materials and welding technology, University of Gent,
B – 9000 Gent

ABSTRACT

An interferometer based on a single multi-functional Holographic Optical Element (HOE) is presented. The interferometer is meant for flatness testing of quite large objects, not necessarily optically polished. Other features include two beam common-path arrangement, desensitization as compared to the classical $\lambda/2$ figure, white-light illumination. Emphasis is then laid on automatic fringe pattern interpretation which makes use of an ad hoc phase-shifting procedure. Results obtained with computer disks are shown.

1. INTRODUCTION

Present trends in quality assessment aim at performing tests as early as possible in the production cycle, in order to avoid to reject objects of high added value, having already undergone expensive processes. At these early stages of manufacturing geometric characteristics may be relatively far from final specifications. This means, for instance, that a flat and smooth object in the finished state may have previously exhibited departure of flatness typically in the range of hundreds of micrometers over dm^2 areas and rms surface roughness of the order of, or greater than the wavelength, making it diffusely reflecting or transmitting.

Both ranges are not so easily accessed by optical methods – too coarse for classical interferometry and still too minute for moiré methods. The methods which are worth considering are reviewed elsewhere[1], but none appears to be fully satisfactory, especially if other features like large dimension, existence of spurious reflections or weak reflection coefficients are also taken into account.

A very simple holographic interferometer has been devised[2-3] in order to overcome most of the above mentioned limitations. The interferometer is first described from a double theoretical and practical point of view. The simplicity of the arrangement is not without counterpoint : due to intrinsic sensitivity variation across the field, automatic interpretation of fringe patterns is not straightforward. Hence the second part of this paper reports a phase-shifting procedure, otherwise of general interest, allowing the automatic measurement of flatness deviation. A five image algorithm solves the problem of sensitivity variation. The algorithm is applied to two interferograms of distinct sensitivity related to the same object. Overabundant data are thus generated. A classical data reduction technique finally gives the unknown values of the air gap thickness between object and hologram. A prototype instrument has been built, allowing to perform experimental verifications and to treat typical examples.

2. DESENSITIZED HOLOGRAPHIC INTERFEROMETER

2.1. Principle

Fig. 1 explains the three main steps leading to the formation of a fringe pattern depicting loci of equal thickness between object and hologram.

A two spherical wave hologram is first recorded, Fig. 1 a, creating on the local scale a line-grating of well established period and orientation. At reconstruction, the illumination beam is diffracted by these elemental gratings, Fig. 1 b. A simple relationship gives the direction of the diffracted beams for any recording and reconstruction geometry and whatever

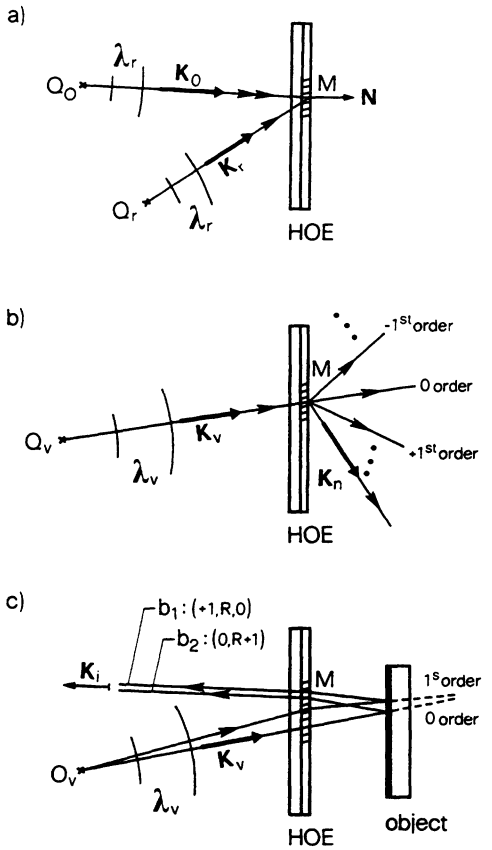

Fig. 1. Principle of the interferometer

the recording, λ_r, and reconstruction, λ_v, wavelengths may be[4] :

$$\mathbf{N} \times (\mathbf{K}_n - \mathbf{K}_v) = n \frac{\lambda_v}{\lambda_r} \mathbf{N} \times (\mathbf{K}_o - \mathbf{K}_r) \tag{1}$$

N is the outside unit normal to the hologram. The hologram is supposed to be recorded with a reference and an object beam of direction $\mathbf{K}_r$ and $\mathbf{K}_o$ respectively and reconstructed by a beam of direction $\mathbf{K}_v$; n is the order of diffraction and $\mathbf{K}_n$ is the direction of the n^{th} diffracted beam. All vectors **K** are unit vectors.

The next step is to place the test object just behind the HOE, Fig. 1c. Of the many diffracted beams, only the zero and first order are of interest. The other beams, propagating in directions far apart, do not participate to the formation of the final interferogram. The zero and first order beams undergo a reflection on the object surface and propagate back to the HOE surface where they are diffracted once more. Again, among the many diffracted beams, only one couple of beams (b_1, b_2) is of interest and serves to form the final interferogram. This pair of beams is defined as follows : b_1 arises from the 0 order diffraction of the beam firstly diffracted into the 1^{st} order; b_2 arises from the 1^{st} order diffraction of the beam firstly transmitted into the 0 order; this can be schematically resumed by :

$$\begin{aligned} &b_1 : (+1, R, 0) \\ &b_2 : (0, R, +1) \end{aligned} \tag{2}$$

where, in chronological order, the numbers denote the diffraction orders and letter R, reflection on the object surface.

A twofold application of Eq. (1) and meanwhile the application of the law of reflection show that beams b_1 and b_2 propagate parallel to each other and into a direction of unit vector $\mathbf{K}_i$ given by :

$$\mathbf{K}_i \left| \begin{aligned} l_i &= l_v + \frac{\lambda_v}{\lambda_r}(l_o - l_r) \\ m_i &= m_v + \frac{\lambda_v}{\lambda_r}(m_o - m_r) \\ n_i &= \sqrt{1 - l_i^2 - m_i^2} \end{aligned} \right. \tag{3}$$

where (l, m, n) are the direction cosines of vectors **K**, with proper and already defined subscripts.

At this point, an important assumption takes place, easily met in practice if the reflecting surface is very close to the HOE surface, namely that the two beams b_1 and b_2 are supposed to leave the hologram at the same point M. The two beams are closer to each other than the spatial resolution limit of the observation system. Hence, the thickness t of the air gap between object and hologram is identical for the two beams :

$$t[b_1] \cong t[b_2] = t(M) \tag{4}$$

This assumption, together with the help of Fig. 2, allows to calculate the optical path difference, δ, between the two

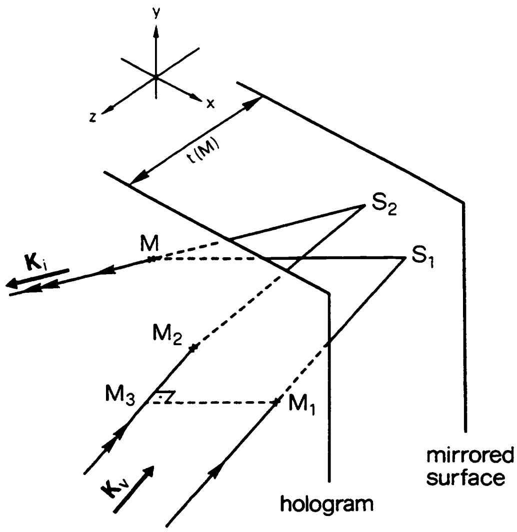

Fig. 2. Optical path difference.

interfering beams (b_1, b_2) :

$$\delta(M) = \frac{2\,t(M)}{\mathbf{K}_i(M)\cdot\mathbf{N}}\left[1+\mathbf{K}_i(M)\cdot\mathbf{K}_v^{'}(M)\right] \tag{5}$$

where $\mathbf{K}_v^{'}$ is the symmetrical of $\mathbf{K}_v$ with respect to the normal $\mathbf{N}$.

Since the amplitudes of the two beams b_1 and b_2 are of the same magnitude, whatever the diffraction efficiency of the hologram and the reflectance of the surface may be, good contrast fringes are produced over the field.

The phase φ of the two beam interferogram is given by :

$$\varphi(M) = \frac{4\pi}{\lambda_v}\frac{t(M)}{\mathbf{K}_i(M)\cdot\mathbf{N}}\left[1+\mathbf{K}_i(M)\cdot\mathbf{K}_v^{'}(M)\right] \tag{6}$$

Lines of equal maximum intensity obey the equation :

$$t_n(M) = \frac{n\lambda_v \mathbf{K}_i(M)\cdot\mathbf{N}}{2\left[1+\mathbf{K}_i(M)\cdot\mathbf{K}_v^{'}(M)\right]} \quad ; \text{ n integer} \tag{7}$$

which allows to calculate the thickness between object and HOE.

Therefore, the sensitivity of the interferometer $s(M,\lambda_v)$ is given by :

$$s(M,\lambda_v) = \frac{2\left[1+\mathbf{K}_i(M)\cdot\mathbf{K}_v^{'}(M)\right]}{\lambda_v\cdot\mathbf{K}_i(M)\cdot\mathbf{N}} \tag{8}$$

In an arrangement where $\mathbf{K}_o$ and $\mathbf{K}_i$ lie on the z-axis and the reference and reconstruction beams are identical ($\mathbf{K}_r = \mathbf{K}_v$) and make an angle θ with the z-axis, Eq. 7 reduces to :

$$t_n(M) = \frac{n\lambda}{2(1-\cos\theta)} \tag{9}$$

More clearly than Eq. 7, this last formula shows that a desensitization factor, σ, given by :

$$\sigma = 1/1-\cos\theta \tag{10}$$

characterizes the operation of the HOE interferometer as compared to the Fizeau arrangement. This factor can approach 100 for small θ angles, illustrating the great flexibility of the interferometer.

2.2. Realization

In order to keep as simple as possible the hypothetical realization of an instrument based on the previous theory, two initial choices are prescribed :

i) no beam shaping or beam splitting components other than the HOE should be added to the system;
ii) white light illumination is highly desirable in order to get rid of much of the coherent noise and for cost purposes.

The first requirement calls for an appropriate use of the holographic conjugation laws[5]. At reconstruction, the illumination wave is spherical divergent. In the paraxial domain the wave diffracted in the 1^{st} order after the 1^{st} passing through the hologram should be spherical convergent. In the same way, the spherical divergent wave, arising from the reflection on the object surface after zero order transmission, should be diffracted into a spherical convergent wave after the second passing through the hologram. Both conditions are indeed identical and can be simultaneously fulfilled. The recording and reconstruction geometries must differ, Fig. 3, but many possibilities are open.

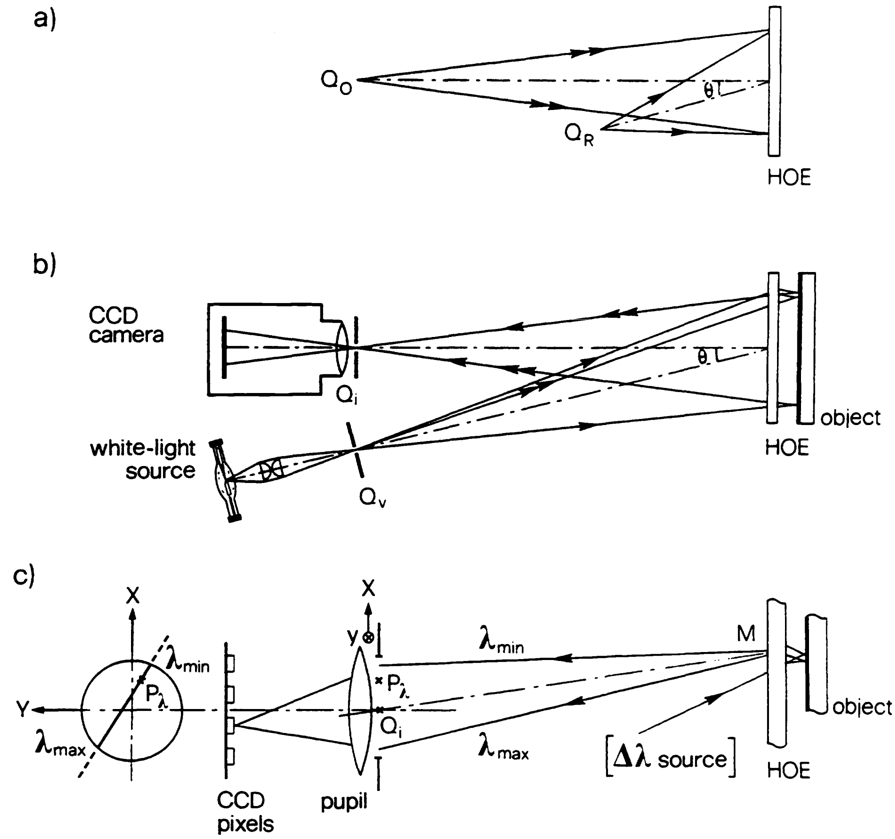

Fig. 3. Geometry of recording and reconstruction.

The most interesting configuration consists in the observation direction lying along the normal to the hologram and drawn from its center. For practical reasons, the distances [center of the pupil of the observation system – hologram] and [object point source – hologram] are the same. In these conditions, the respective distances sources-hologram, ρ, obey the following equation :

$$\frac{1}{\rho_v} = \frac{1}{\rho_r} - \left(\frac{1}{\rho_i} + \frac{1}{\rho_o}\right) \qquad (11)$$

where subscripts v, r, i, o have the same meaning as previously. In this arrangement, paraxial rays of the same wavelength as that of the recording focus at the center of the pupil of the observation system.

White light reconstruction brings about an additional effect related to the chromatic dispersion of the HOE. Holographic conjugation laws warn that the focus Q_i can be considerably enlarged by chromatic aberrations. Any ray impinging on the HOE will suffer a wavelength dependent angular deflection given by Eq. 1, where the reconstruction wavelength λ_v belongs now to the interval defining the source spectrum. On the return, only a definite number of these rays will fall inside the pupil of the observation system. This means that each image point possesses a certain spectral content, which is changing over the field. Both effects have to be known precisely, due to the wavelength dependence of the optical path difference, Eq. (5) and, hence, of the sensitivity, Eq. (8).

The finite range of spectral components accepted by the pupil for image formation on any pixel of the detector has first to be determined.

In a coordinate system (X,Y) belonging to the plane of the pupil and with origin at the center of the pupil, Fig. 3 c, the coordinates (X_λ, Y_λ) of the ray intersections are given by :

$$P_\lambda \left| \begin{array}{l} X_\lambda = x + \rho_i \dfrac{l_i}{n_i} \\ Y_\lambda = y + \rho_i \dfrac{m_i}{n_i} \end{array} \right. \qquad (12)$$

In Eq. (12), (x, y) are the coordinates of the HOE point where the ray leaves the hologram; ρ_i, the distance pupil-hologram, is calculated by Eq. (11) and (l_i, m_i, n_i) are the direction cosines of vector $\mathbf{K_i}$, calculated using Eq. (3). The wavelength dependence is explicit through this last equation.

A computer program allows to calculate the coordinates of P_λ, for any ray leaving the hologram, in an arbitrary pair of recording and reconstruction geometry and, all parameters otherwise fixed, to scan the complete spectral range of the source. For each point M of the HOE two additional calculations are performed:

i) the limits of the wavelength range admitted by the pupil are determined. These limits (λ_{min}, λ_{max}) are solutions of the equation :

$$X_\lambda^2 + Y_\lambda^2 = Rp^2 \tag{13}$$

where R_p designates the radius of the pupil.

ii) the sensitivity, s(λ, M), according to Eq. (8), for each spectral component admitted by the pupil.

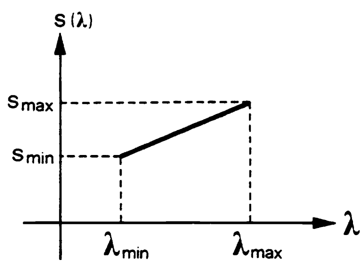

Fig. 4. Wavelength dependence of the sensitivity.

For all the tested configurations of practical interest, the sensitivity appears to be a linear function of the wavelength, for values taken inside the interval of wavelength admitted by the pupil, Fig. 4 :

$$s(\lambda;M) = \alpha + \beta\lambda \quad ; \quad \lambda \in [\lambda_{min}, \lambda_{max}] \tag{14}$$

Another interesting result, provided by the program and consistent with the holographic conjugation laws, is as follows : the ray intersections with the pupil plane are evenly distributed along a straight line when the spectral range is scanned.

These two results have an important consequence : the intensity, I_I, spatially integrated over each pixel of the receptor, can be expressed by :

$$I_I(M) = \int_{\lambda_{min}}^{\lambda_{max}} I(\lambda, M)\, d\lambda \tag{15}$$

where $I(\lambda, M)$ represents the classical intensity profile of a two beam interference pattern of contrast V and mean intensity I_o :

$$I(\lambda, M) = I_o\left[1 + V\cos\left(2\pi s(\lambda, M)\, t(M)\right)\right] \tag{16}$$

Substituting into Eq. (16) the linear expression for the sensitivity and performing the integration leave :

$$I_I(\lambda, M) \equiv I_I\left(\bar{\lambda}, M\right) = I'_o\left[1 + V' \cos 2\pi\left(\alpha + \beta\bar{\lambda}\right)t(M)\right] \tag{17a}$$

where

$$V' = V \sin_c \beta\Delta\lambda t(M) \tag{17b}$$

and

$$\bar{\lambda} = \frac{\lambda_{max} + \lambda_{min}}{2} \quad ; \quad \Delta\lambda = \lambda_{max} - \lambda_{min} \tag{17c}$$

In other words, a two beam equivalent interference pattern is obtained, with reduced contrast V' and equivalent wavelength equal to the arithmetic mean between the two extreme wavelengths admitted by the pupil. This mean wavelength is also the wavelength of the ray which intersects the pupil in the middle of the line defined by all the other and differently coloured intersections. Typical values of $\Delta\lambda$, t(M) and β are respectively smaller than 25nm, 100μm and 0.1μm^{-2}, so that the contrast remains always above 50 %.

The sensitivity in each pixel of the image field :

$$s(\lambda,M) \equiv s(\bar{\lambda},M) = \alpha + \beta\bar{\lambda} \tag{18}$$

can be simply calculated by means of Eq. (8), in which the wavelength λ_V is replaced by the mean wavelength $\bar{\lambda}$ directly deduced from Eq. (13).

Eqs (17) provide the complete significance of the fringe pattern obtained by white light illumination of the interferometer and the only problem left is the automatic interpretation of these fringe patterns; but, before to tackle this question a brief summary of the advantages and main properties of the interferometer is given.

2.3. Properties

Immediately after the possibilities to desensitize the interferograms and to examine objects non optically polished, the next main characteristic of the interferometer is its simplicity. A single HOE fulfils on its own all the functions devoted to the interferometer : beam-division, -deflection, -recombination, -focusing. Better still, the HOE provides a reference of flatness and performs the necessary chromatic filtering when the interferometer is illuminated with white light. As the result of recording a two beam interference pattern between spherical divergent waves, the realization of the HOE is particularly simple, even for several dm^2 plates. Possibilities of duplication render this element very flexible and inexpensive. The only other components are a small halogen spot light and a B&W CCD camera. Reconstruction is free from coherent noise. Limited coherence length of the source may be used also to eliminate the influence of the reflection from the rear face of a transparent object : the pupil of the observation system has simply to be open until the contrast of the rear face interferogram falls to zero, according to Eq. (17b). Due to HOE focusing properties, luminous flux collection is very good and the light yield is very high. The object is observed along its normal, an advantage not shared by obliquely desensitized interferometers.

Being of common-path type, the interferometer is easy to adjust and benefit from excellent stability conditions. The contrast of the interferogram is intrinsically high because the two waves possess identical amplitudes : both undergo a first order diffraction, a zero order transmission and a reflection at the object surface. The reflectance of the object surface has indeed no influence on the fringe contrast. This is an additional advantage, not encountered in classical interferometry where the coating of the reference component must be adapted to the reflectance of the tested object.

Finally the interferometer is amenable to an automatic readout system by using phase-shifting techniques, as presented below.

3. AUTOMATIC INTERPRETATION PROCEDURE

Phase-shifting techniques are known to be very powerful and accurate tools for quasi-parallel automatic interpretation of fringe patterns[6,7]. The sole practical difficulty lies in the necessity to freeze the unknown phase during the time needed to acquire a given number of phase-shifted versions of the interferogram. This can be difficult to achieve in dynamic strain analysis, but, as far as shape measurements are concerned, the requirement is easily fulfilled. Therefore the choice was to rely on these techniques.

However, the interferometer is of the common-path type and the only way to increment the phase of the interferogram is to change stepwise the mean distance object-hologram, e.g. by translating the hologram perpendicular to its plane. If Δt designates the thickness change produced by such a translation, the resultant phase-shift, α, is given by :

$$\alpha(M) = \frac{4\pi}{\bar{\lambda}(M)} \frac{\left(1 + \mathbf{K}_i(M)\cdot \mathbf{K}_v'(M)\right)}{\mathbf{K}_i(M)\cdot \mathbf{N}} \Delta t \tag{19}$$

This shift is not uniform over the field. Moreover and contrary to the rule applying to most of the classical interferometers, the knowledge of the phase is no longer equivalent to the knowledge of the distance object-hologram.

Solving these two problems calls for a special procedure.

3.1. Five-image algorithm

An analytical expression for the phase, φ, of a two beam interference pattern can be obtained as soon as 3 equiphase shifted versions of the same interferogram are available. For example, by denoting I_1, I_2, I_3 the three intensity distributions corresponding to the phase-shifts $-\alpha$, 0, $+\alpha$, the inversion formula is given by :

$$\varphi = \tan^{-1}\left[\left(\frac{1-\cos\alpha}{\sin\alpha}\right)\frac{I_1 - I_3}{2I_2 - I_1 - I_3}\right] \tag{20}$$

Although possible, this algorithm is not well adapted to the HOE interferometer, for one should first calculate the exact amount of phase step realized in each pixel of the field, according to Eq. (19). Calibration procedure would be tedious, leading to poor final precision.

In the case of a stationary phase as many shifted versions as needed of the same pattern can be recorded and a 4-image algorithm comes next into consideration. The supernumerary equation serves to eliminate the unknown value of the carried out phase step, provided that the steps are evenly spaced. The four intensity distributions I_1 to I_4, give directly the value of the unknown phase by :

$$\varphi = \tan^{-1}\left[\frac{\sqrt{(I_1 - I_4 + I_2 - I_3)[3(I_2 - I_3)] - I_1 + I_4}}{(I_2 + I_3) - (I_1 + I_4)}\right] \tag{21}$$

Introducing the same phase-shift for each new step at any point of the field is simply achieved by translating the hologram as a whole (or the object) by equal amounts, normally to its surface, no matter how much these translations really are. Contrary to the previous algorithm, calculations involving many geometric data are bypassed. Unfortunately, the 4-image algorithm behaves rather poorly for phase values equal to integer multiples of π.

The 5-image algorithm with arbitrary equispaced phase-shifts does not suffer from the latter drawback, while retaining all the other advantages of the 4-image algorithm. This algorithm gives the phase according to the following relations :

$$\begin{cases} I_i(M) = I(M)\left[1 + V(M)\cos(\varphi(M) + (i-3)\alpha(M))\right] \quad ; \quad i \in \{1,2,3,4,5\} \\ \alpha(M) = \cos^{-1}\left[\dfrac{I_5(M) - I_1(M)}{2(I_4(M) - I_2(M))}\right] \\ \varphi(M) = \tan^{-1}\left[\dfrac{2(I_2(M) - I_4(M))}{2I_3(M) - I_5(M) - I_1(M)}\sin\alpha(M)\right] \end{cases} \tag{22}$$

This algorithm solves the problem of the non-uniform shift over the field. The constant value of the thickness increment is chosen in order that the phase-shift is $\pi/2$ at the centre of the field - a value for which the 5-image algorithm is the most insensitive and consequently the most tolerant to small errors possibly impairing the realization of the shifts. Using Eq. (22), a computer program provides firstly the wrapped phase map of the interferogram, i.e. the principal determination between 0 and 2π of the inverse tangent. Then the phase is automatically unwrapped by searching, on a local basis, for phase jumps of the order of 2π. At the end of this second operation, the numerical value of the phase is known at every point M of the field up to an arbitrary additive constant k :

$$\varphi(M) = 2\pi s(M)t(M) + 2k\pi \tag{23}$$

3.2. Two interferograms

In a constant sensitivity interferometer, Eq. (23) would already represent the result of the measurement as the knowledge of the thickness object - reference surface up to a constant gap is a sufficient information : the interest being to measure the shape of the object, the additional gap is irrelevant since it corresponds to a translation perpendicularly to itself of the reference plane.

In the case of sensitivity variation across the field the knowledge of the phase is no longer equivalent to the knowledge of the thickness object - hologram. The shape of the object can be obtained only after elimination of the arbitrary constant in Eq. (23). In principle, it suffices to know the thickness at one location of the interferogram and the condition of mechanical contact between object and hologram, mediated for instance by one or several calibrated spacers, could bring the solution.

However, a pure optical non-contacting method is preferable. The lacking information can be extracted from a second interferogram and the same HOE can easily handle this new possibility. Instead of two beams, recording of the HOE is performed with three beams : the so-called object beam, as previously, and two reference beams angularly separated. Upon reconstruction, two white light sources take the place of the reference beams. By illuminating object and hologram successively by each of these sources, two distinct interferograms are displayed. Obviously, the phase of each one can be calculated as in section (3.1). In n points $\{(M_1,\ldots,M_i,\ldots,M_n)\}$ of the interferogram, 2n distinct values of the phase are known :

$$\begin{cases} \varphi_1(M_i) = 2\pi s_1(M_i)t(M_i) + 2\pi k_1 \\ \varphi_2(M_i) = 2\pi s_2(M_i)t(M_i) + 2\pi k_2 \end{cases} \tag{24}$$

where subscripts 1 and 2 refer to the corresponding interferograms and sensitivities. Eq. (24) represents a linear system of 2n equations and n + 2 unknowns, which can be solved by a least squares technique as soon as n is greater than 2.

3.3. Data reduction

Eq. (24) can be regarded as the definition of a line D_i in (k_1, k_2) space, after elimination of $t(M_i)$:

$$\begin{cases} a_i k_1 + b_i k_2 + c_i = 0 \\ a_i = s_2(M_i) \quad ; \quad b_i = s_1(M_i) \quad ; \quad c_i = \dfrac{1}{2\pi}\left[s_1(M_i)\varphi_2(M_i) - s_2(M_i)\varphi_1(M_i)\right] \end{cases} \tag{25}$$

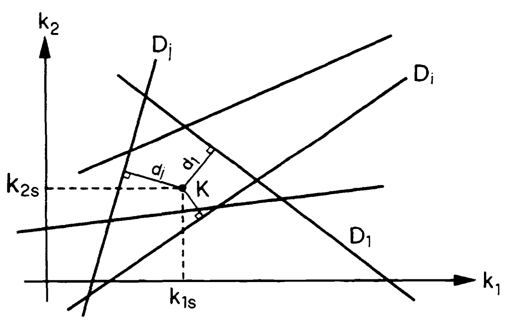

Fig. 5. Geometric representation of Eq. (24).

Lines such as D_i are represented in Fig. 5. In an ideal measurement system, all lines would intersect at a single point K and the coordinates of K would be the solution for the arbitrary constants k_1 and k_2. Due to measurement errors, many intersections between the D_i lines exist. However one can still calculate the coordinates (k_{1s}, k_{2s}) of a point K lying at the closest cumulated distance to all the D_i lines, representing the solution. Mathematically, this simply consists in equating to zero the partial derivatives of the sum of the squared distances (d_i^2) with respect to k_1 and k_2 and in solving the resulting system of two equations, linear in k_1, k_2.

A program is implemented which allows to compute the values (k_{1s}, k_{2s}), taking into account a chosen number n of measurement points. Finally, the thickness between object and hologram at any point of the field is given by :

$$t(M_i) = \frac{1}{4\pi}\left[\frac{\varphi_1(M_i) - 2\pi k_{1s}}{s_1(M_i)} + \frac{\varphi_2(M_i) - 2\pi k_{2s}}{s_2(M_i)}\right] \tag{26}$$

which represents the arithmetic mean of the two existing solutions.

Hence a phase-shifting software, successively run for two distinct interferograms related to the same object and followed by a least squares technique for data reduction, provides a fully automatic quantitative interpretation of the fringe patterns. The procedure is first applied to an optical flat in order to measure the flatness deviation of the HOE itself. The corresponding figure is stored once and for all in the computer and systematically subtracted from the figures resulting of Eq. (26) for objects currently under examination. The absolute shape of the tested object is thus determined and the desensitized interferometer meets an interesting trend in present day interferometry : the computer alleviates the necessity for a perfect reference surface to be physically present in each interferometer. It becomes sufficient to accurately calibrate the reference component.

Although specifically developed for a custom device, the method described in the present section is applicable to many other interferometers.

4. APPLICATION

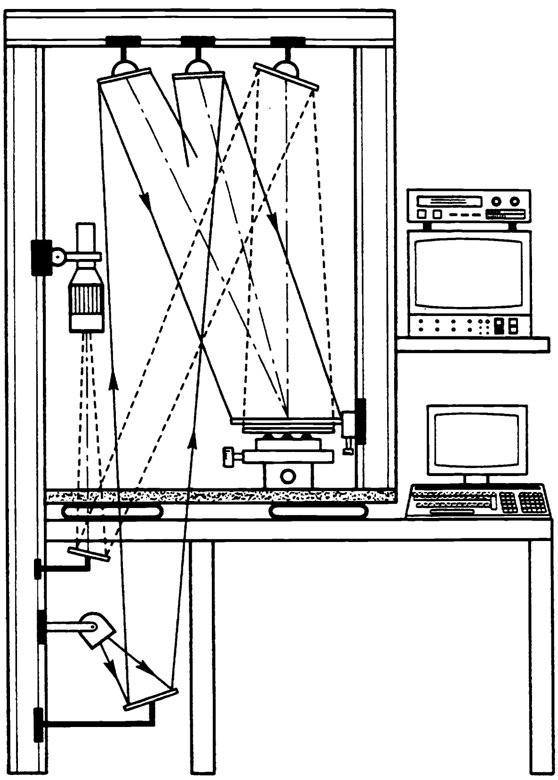

Fig. 6. Sketch of the prototype.

A prototype of the instrument has been built, Fig. 6. A good compromise between the contradictory requirements of large distance source - hologram and limited dimensions has been found by fixing all the components of the interferometer on a vertical U-shaped bench upside down. The frame is about 2m high and 1m wide.

A single 50W halogen lamp is divided into two sources by means of a bi-mirror arrangement and gives rise to two illumination directions of the HOE, under the mean incidence angles of 14^o and 26^o respectively. The 8x10" hologram is recorded with the 647nm krypton laser line. Taking into account the recording geometry, the nominal sensitivity at the centre of the field is respectively 10.8μm and 3.1μm per fringe for the two illumination directions. The sensitivity variation from the centre to the border of the field, 65mm apart, amounts to 45% and 17% respectively. The object, placed just behind the hologram, is observed normally.

The interferometer is first adjusted by using the same wavelength than that of the recording. Reticles drawn on the hologram at locations accurately known serve to calibrate the inter pixel distances of the CCD camera, both horizontally and vertically, in term of real dimension of the object surface. The distance object-hologram can be precisely changed by actuating a PZT pusher under computer control, which realizes the needed phase-shifts. In the actual state, the system is equipped with a standard video acquisition board of 512x512 pixels, digitized to 8 bits.

All steps of the phase-shifting acquisitions and calculations are completely automated, as well as the additional operations of absolute shape determination.

Fig. 7 shows 2 of the 5 phase shifted fringe patterns obtained for the highest sensitivity of 3.1μm per fringe. The object is a 5" aluminium computer disk in the early stage of manufacturing. The sample is optically diffusing, as expected from a surface roughness of the order of the wavelength or greater. Nevertheless, the wrapped phase map does not exhibit pepper noise effects, as usually observed with rough surfaces in speckle interferometry. Therefore, phase unwrapping can be performed quite easily and relies on a simple algorithm based on local search for 2π phase jumps.

Fig. 8 shows the same steps related to the same object, but for the second sensitivity of 10.8μm per fringe.

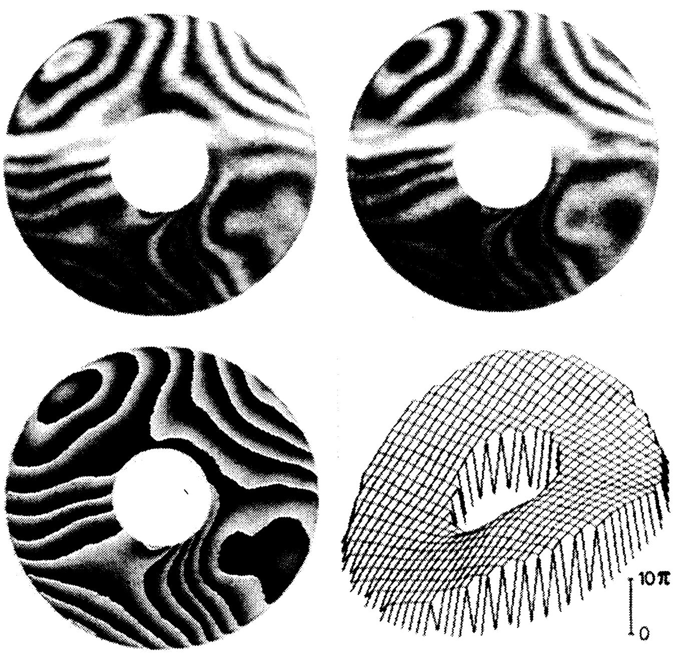

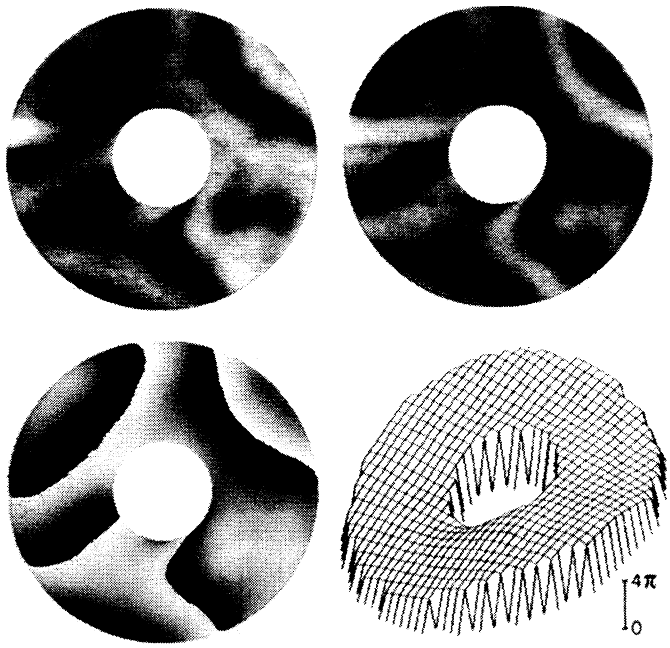

Fig. 7. Phase calculation related to a rough computer disk. Sensitivity of 3.1 micron per fringe.

Fig. 8. Phase calculation for the same object as in Fig. 7. Sensitivity of 10.8 micron per fringe.

Fig. 9 illustrates the final result. The flatness deviation of the hologram has first been calculated by following the procedure described in sections 3.1, 3.2 and 3.3, in which the object is a mirror of excellent figure. Fig. 9a displays the shape of the hologram.

From the results shown in Fig. 7d and 8d, and after performing the operations of section 3.3, the thickness between disk and hologram is obtained and represented in Fig. 9b. After correction for the deviation of the hologram, Fig. 9c represents the absolute shape of the disk.

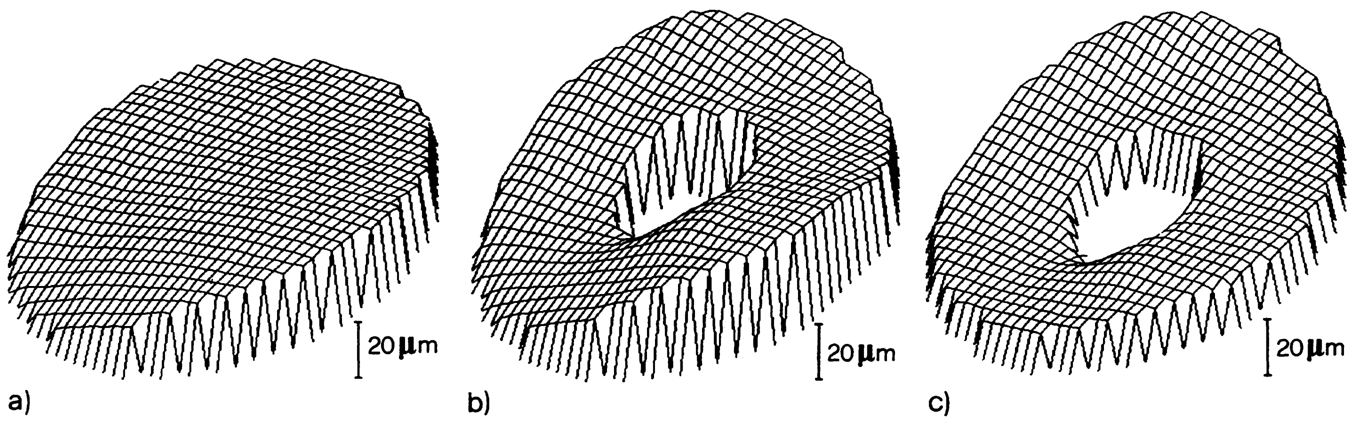

Fig. 9. From left to right: flatness deviation of the HOE; thickness between disk and HOE; flatness deviation of the disk.

The system has capabilities to furnish 512x512 height data with a precision better than 0.5μm over a measurement range of several hundreds of microns. As yet, the duration of a complete measurement has not been optimized and takes several minutes.

5. CONCLUSION

The all-holographic, white light, desensitized common-path interferometer presented here has been devised with the aim to cover an important measurement domain of great technological significance, otherwise poorly treated by classical methods : the measurement of flatness departure of quite large objects, mechanically smooth but not necessarily optically polished, in the height range of 1 to several hundreds of μm. Simplicity is one of the key feature of this interferometer. Problems posed by automatic fringe pattern interpretation and arising mainly from the sensitivity variation across the field have been completely solved by relying on the powerful phase-shifting techniques. Consequently, the prototype built for feasibility purpose is very close to an industrial instrument.

ACKNOWLEDGEMENTS

The assistance of Isabelle Vouilloz, Raymond Délez and Jean-Louis Guignard is greatly acknowledged. The participation of Alban L'Herminé and Marc Leconte of the Ecole Supérieure d'Optique, Orsay, in the frame of their practical diploma works, to the phase of prototype realization has been much appreciated. P.B. gratefully acknowledges the support of the Belgian National Foundation for Scientific Research through grant 200 44 86.

REFERENCES

1. P. Jacquot and P.M. Boone, "Deux méthodes holographiques appliquées au contrôle de planéité", Opto 1988, ESI publications, Paris, pp. 313-319 (1988).
2. P. Jacquot and P.M. Boone, "Two holographic methods for flatness testing with sub-wavelength or multiple wavelength sensitivities", SPIE vol. 1212, Practical Holography IV, pp. 207-219 (1990).
3. P.M. Boone and P. Jacquot, "Some application of a HOE based desensitized interferometer in materials research, SPIE vol. 1554 A, Photomechanics and speckle metrology, pp. 512-521 (1991).
4. W.T. Welford, "A vector ray tracing equation for hologram lenses of arbitrary shape", Optics Comm., 14, pp. 322-323 (1975).
5. E.B. Champagne, "Non paraxial imaging, magnification and aberrations properties in holography", J. Opt. Soc. Am., 57, pp. 51-55 (1967).
6. D.W. Robinson and G.T. Reid (Eds), "Interferogram analysis : digital fringe pattern measurement techniques", Institute of Physics Publishing, 1993.
7. W. Jüptner and W. Osten (Eds), "Fringe '93", Akademie Verlag, 1993.